Geophysical Journal International

*Geophys. J. Int.* (2011) **186,** 760–770 doi: 10.1111/j.1365-246X.2011.05055.x

# Seismic structures of the Calico fault zone inferred from local earthquake travel time modelling

Hongfeng Yang,[1,2] Lupei Zhu[1] and Elizabeth S. Cochran[3]

[1] *Department of Earth and Atmospheric Sciences, Saint Louis University, St Louis,* MO 63108, *USA. E-mail: hyang@whoi.edu*
[2] *Department of Geology and Geophysics, Woods Hole Oceanographic Institution, Woods Hole,* MA 02543, *USA*
[3] *Department of Earth Sciences, University of California, Riverside,* CA 92521, *USA*

Accepted 2011 April 26. Received 2011 April 26; in original form 2011 January 18

## SUMMARY

We analysed high-frequency body waves of local earthquakes to image the damage zone of the Calico fault in the eastern California shear zone. We used generalized ray theory and finite difference methods to compute synthetic seismograms for a low-velocity fault zone (FZ) to model the direct and FZ-reflected *P* and *S* traveltimes of local earthquakes recorded by a temporary array across the fault. The low velocity zone boundaries were determined by apparent traveltime delays across the fault. The velocity contrast between the fault zone and host rock was constrained by the traveltime delays of *P* and *S* waves and differential traveltimes between the direct and FZ-reflected waves. The dip and depth extent of the low velocity zone were constrained by a systematic analysis of direct *P* traveltimes of events on both sides of the fault. We found that the Calico fault has a ∼1.3-km-wide low velocity zone in which the *P*- and *S*-wave velocity decreased 40 and 50 per cent, respectively, with respect to the host rock. The low velocity zone dips 70° northeast and extends 3 km in depth.

**Key words:** Body waves; Interface waves; Wave propagation.



## 1 INTRODUCTION

Crustal faults are usually associated with a damage zone of hundreds of metres to several kilometres in width with significantly reduced seismic velocities and rigidity compared to the host rock (e.g. Li *et al.* 1990; Chester *et al.* 1993; Evans & Chester 1995; Fialko *et al.* 2002; Rovelli *et al.* 2002; Ben-Zion *et al.* 2003). The damage zone is composed of highly fractured materials, breccia, clay and cataclasites, and is seismically characterized as a low velocity zone (LVZ; e.g. Chester & Logan 1986; Ben-Zion & Sammis 2003, 2009). Cracks in the damage zone may contain and transport fluids which play an important role on fault zone strength related to earthquake generation and rupture distribution (Eberhart-Phillips *et al.* 1995). Experimental studies of off-fault damage point out that the LVZ can have strong effects on earthquake rupture propagation and rupture speed (Sammis *et al.* 2009), that is also confirmed by a recent numerical study of the effect on dynamic rupture properties of the LVZ (Huang & Ampuero 2010). The LVZ may amplify the ground motion by a factor larger than 10 (Ben-Zion & Aki 1990), may reflect asymmetric damage generation during earthquakes (e.g. Ben-Zion & Shi 2005; Dor *et al.* 2006), and could cause anomalous coseismic deformations (e.g. Fialko *et al.* 2002; Hearn & Fialko 2009; Duan 2010). Investigations of generation and healing of FZ damage immediately after the occurrence of large earthquakes show rapid processes (Peng & Ben-Zion 2006; Wu *et al.* 2009) that reflect the opening and closing of cracks in the FZ rocks, therefore provide information on rock rheology. Studies of temporal velocity variation of LVZ and damage zone healing in the years to decades following a large earthquake highlight its importance to understanding earthquake cycle and evolution of fault systems (Li *et al.* 1998; Vidale & Li 2003). Many fault zone (FZ) related studies suggest that the LVZ structure may control mechanics of earthquake rupture, localization of strain, and is important to understanding the earthquake physics (e.g. Aki 1979; Scholz 1990; Kanamori 1994; Kanamori & Brodsky 2004).

Many geological and geophysical methods have been used to determine FZ structures, including direct analysis of FZ samples (Chester *et al.* 1993; Evans & Chester 1995), modelling fracture densities in the LVZ (Schulz & Evans 1998; Savage & Brodsky 2011), and imaging seismic structures of the FZ using earthquake locations and seismic waves (Li *et al.* 1990, 2000; Ben-Zion *et al.* 2003; McGuire & Ben-Zion 2005; Li *et al.* 2007; Zhao & Peng 2008; Zhang *et al.* 2009; Yang *et al.* 2009). So far the most frequently used method is the so-called FZ trapped waves (Li *et al.* 1990, 2000; Ben-Zion *et al.* 2003), which have been used to determine seismic structures of the LVZ of many faults. Most trapped wave studies have suggested that the LVZ of faults are a few hundred metres wide and with seismic velocity reduction of 20–50 per cent (Li & Vernon 2001; Ben-Zion *et al.* 2003; Lewis *et al.* 2005). However, it is still under debate whether the trapped energy comes from a shallow LVZ structure (e.g. 2–5 km) or from a LVZ that extends to greater depths (Li *et al.* 1997; Li & Vernon 2001; Ben-Zion & Sammis 2003; Lewis *et al.* 2005). For example, a 15–20-km-deep LVZ along the San Jacinto FZ was reported (Li & Vernon 2001) while groups

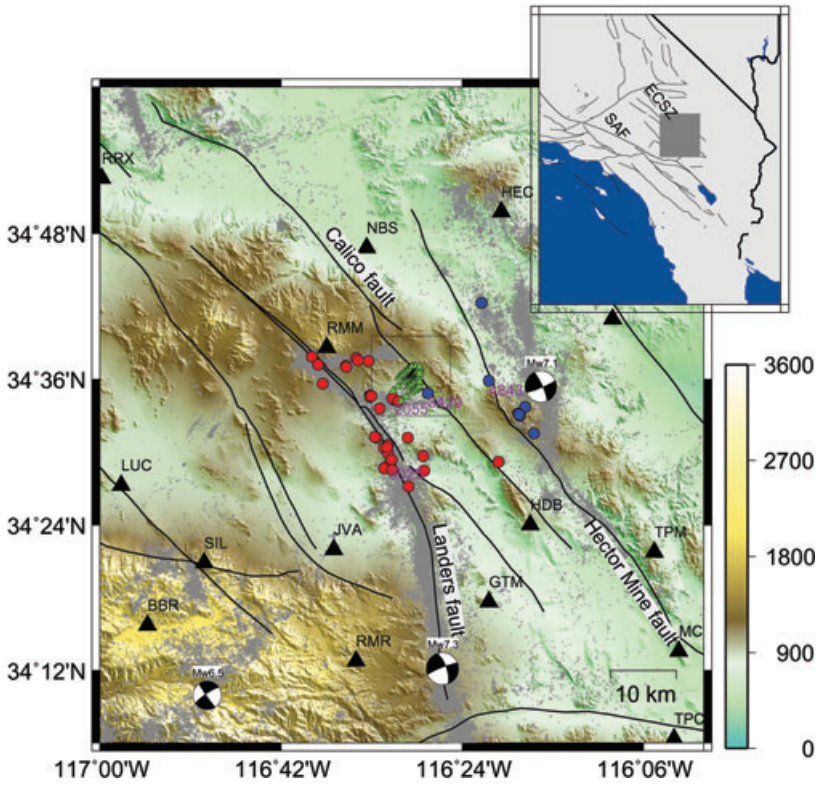


**Figure 1.** Map showing the Calico fault and nearby major earthquakes (beach balls), faults (black lines), and seismicity since 1981 (grey crosses). Triangles are the temporary array (green) deployed in 2006 and permanent stations (black) in the region. Earthquakes used in this study are shown by dots of which blue and red colours represent positive and negative *P*-wave traveltime differences between the northeastern most and southwestern most stations of the array, respectively. Inset figure is a map showing location of study region. SAF, San Andreas fault; ECSZ, eastern California shear zone.

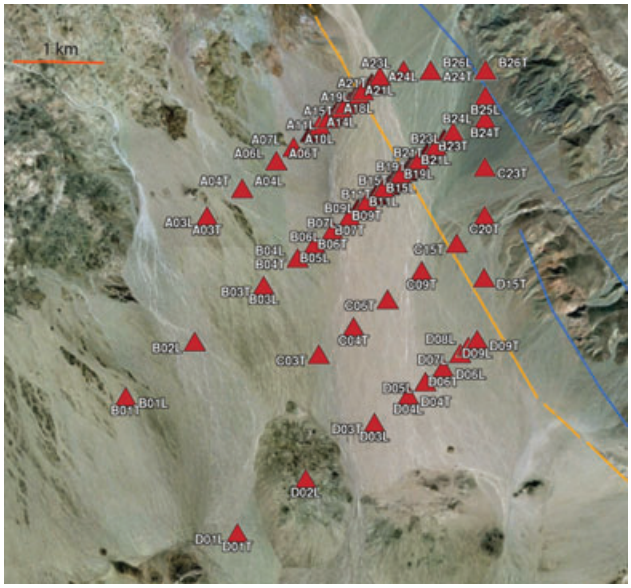


**Figure 2.** Red triangles stand for the temporary array. Two segments of the Calico fault are shown near the array. Orange indicates Holocene faults and blue is Quaternary (U.S. Geological Survey & California Geological Survey 2006).

using the same data set argued that it is limited to the upper 2–5 km deep (Lewis *et al.* 2005; Yang & Zhu 2010b). The depth extent of the damage zone of the San Andreas fault (SAF) at Parkfield was estimated to extend to ∼5 km (Li *et al.* 2004), while a recent study suggested a >10 km low velocity waveguide (Wu *et al.* 2010). Moreover, another group performed a comprehensive analysis of trapped waves and suggested a shallow damage structure, ∼3 km, and they found an incoherent trapping structure along the strike of the fault (Lewis & Ben-Zion 2010).

The damage zone of the Calico fault was estimated to be 1.5–2.0 km wide with a 50 per cent reduction in *S*-wave velocity and elastic moduli based on FZ trapped waves and high resolution Interferometric Synthetic Aperture Radar data (Fialko *et al.* 2002; Cochran *et al.* 2009). This is much wider than LVZ widths of other FZs and it was also suggested that the Calico fault damage zone might persist for hundreds to thousands of years since the last fault rupture. The depth of the LVZ was constrained to at least 5 km, with suggestion of a weak LVZ up to a depth of 12 km that was constrained by waveform modelling of a single deep event assuming the LVZ is vertical (Cochran *et al.* 2009). Recent investigations reported dipping LVZs, for example, the Calico fault (Yang & Zhu 2010a) and the San Jacinto fault (Yang & Zhu 2010b). Ignoring FZ dip could cause large error in estimating the depth extent of the LVZ even other FZ parameters are well constrained (Li *et al.* 2007). Therefore, more detailed studies of the damage zone structure of the Calico fault would be valuable. In this study, we perform a systematic analysis of body waves from all available local earthquakes near the Calico fault to probe fine structures of the FZ. Using a recently developed technique (Li *et al.* 2007), which can significantly reduce the trade-offs among FZ parameters, we determine the LVZ width and seismic velocity reductions of the damaged fault. In our previous study of the San Jacinto FZ, we determined the FZ dip by analysing differential arrival times of *P* waves across the FZ before

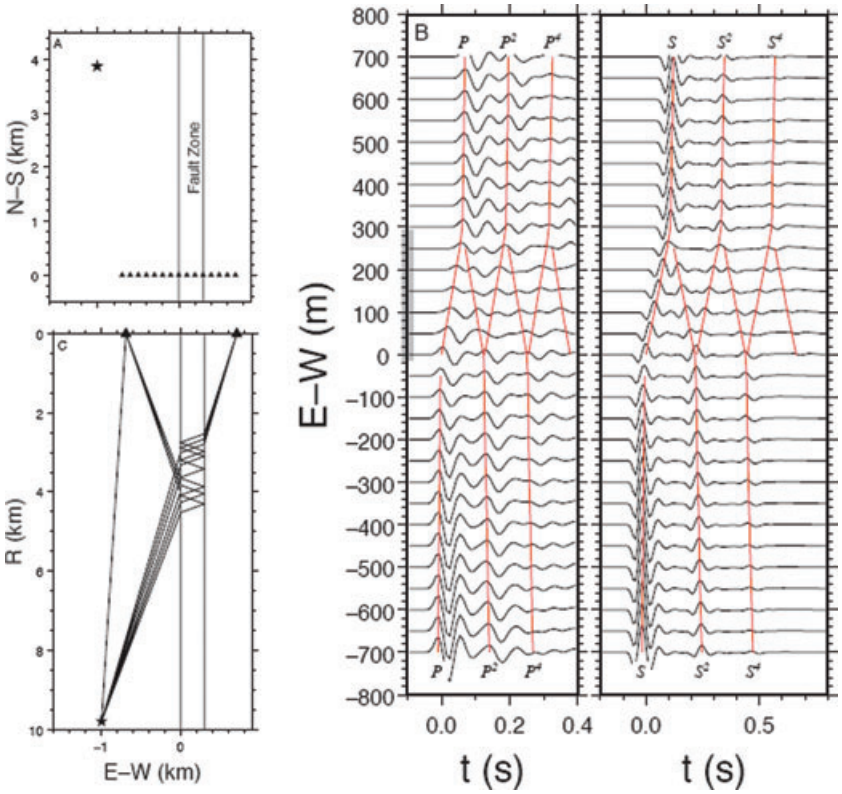


**Figure 3.** Model results for a hypothetical 300-m-wide fault zone. (a) Location of a linear seismic array (triangles) across a 300-m-wide FZ. The earthquake (star) is located 1 km west to the western FZ boundary. (b) The vertical (left-hand panel) and fault-parallel (right-hand panel) components of synthetic seismograms from the linear array. The grey bar represents location of the FZ. Red lines show arrival times of major body-wave phases. Their ray paths to two stations are shown in (c). After (Li *et al.* 2007).

determining the depth extent of LVZ (Yang & Zhu 2010b). Such two-step analysis is not applicable for the Calico fault because gaps in earthquake distribution lead to a trade-off between the dip and the depth extent of the LVZ. Here we determine the FZ dip and depth extent simultaneously by using *P*-wave traveltimes of events on both sides of the FZ. Finally, we summarize the fine structures of the Calico FZ from modelling high frequency body-wave traveltimes of local earthquakes.

## 2 TECTONIC SETTING AND DATA

The Calico fault is located in the eastern California shear zone (ECSZ) which accounts for 9–14 per cent of the total shear along the Pacific–North American transform boundary since ∼10.6 Ma (Dokka & Travis 1990; McClusky *et al.* 2001). It is one of a family of dextral faults that traverse the Mojave Desert portion of the ECSZ and has accumulated ∼10 km of dextral slip since its inception (Oskin *et al.* 2007). Initiation of movement along the fault likely occurred between ∼10 and 6 Ma, and was probably related to Pacific-North American plate interaction (Dokka & Travis 1990). A recent study has determined the average slip rate of the Calico fault as 1.4–1.8 mm yr$^{-1}$ by mapping Pleistocene alluvial fan deposits and $^{40}$Ar /$^{39}$Ar dating (Oskin *et al.* 2007). The northern portion of the Calico fault connects to the Blackwater fault and ends in the south of the northeast-trending Garlock fault. The southern portion of the Calico fault lies between the ruptured faults of the 1992 $M_w$ 7.3 Landers and the 1999 $M_w$ 7.1 Hector Mine earthquakes (Fig. 1). The Calico fault damage zone suffered twice as much strain as the surrounding host rock during these two earthquakes (Fialko *et al.* 2002; Simons *et al.* 2002).

To investigate the Calico FZ structures, a dense array of 100 seismometers was installed across the fault in 2006 June (Cochran *et al.* 2009). The temporary array consists of 40 intermediate-period and 60 short-period (L22 2 Hz) seismometers in a 1.5 km × 5.5 km grid adjacent to the Calico fault (Fig. 2). The instruments had been continuously operated in the field for 6 months. We obtained waveform data of 35 local earthquakes with epicentral distance less than 18 km to the reference station (B20) of the array. Most of the earthquakes are located in the Landers and Hector Mine aftershock zones, and only two of them are located in the Calico FZ (Fig. 1). They are all small events with magnitudes ranging from 0.7 to 3.0 in the Southern California Earthquake Center (SCEC) catalogue. We obtained their locations from Hauksson (2010, personal communication), who relocated earthquakes of southern California using a 3-D velocity model. Event location uncertainties are less than 1 km in lateral distance. We further improved the event focal depths using their *S*–*P* times at the temporary array.

## 3 DATA ANALYSIS AND RESULTS

We removed instrument responses of the ground velocity waveforms and applied a Butterworth bandpass filter between 1 and 10 Hz. We then hand picked *P*- and *S*-wave arrivals for each local earthquake. To study the structures of the Calico FZ using the newly developed technique of Li *et al.* (2007), we selected the longest profile, B, in the temporary array and set up the coordinate origin at a reference station (B20). We rotated three component seismograms of

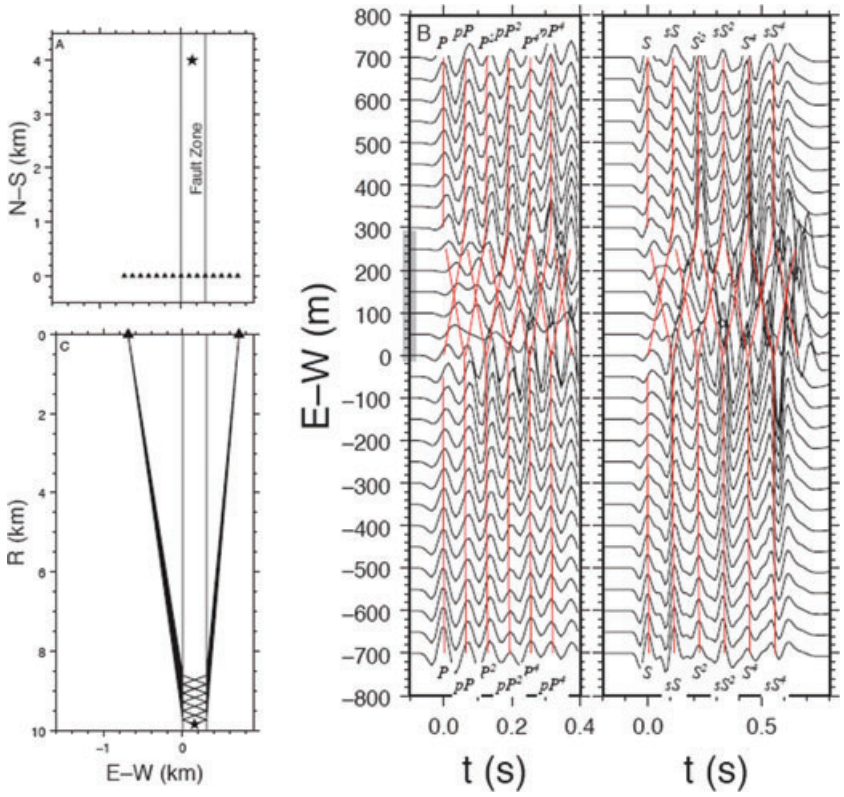


**Figure 4.** Same as Fig. 3, except the earthquake is located in the FZ. After (Li *et al.* 2007).

earthquakes into the FZ radial, FZ normal and FZ parallel directions (see details in Li *et al.* 2007) using the strike of the surface fault trace (N50W) and a vertical FZ assumption (Cochran *et al.* 2009).

### 3.1 LVZ width and velocity drops

Recently, we developed a technique to determine high-resolution FZ structures using arrival times of FZ transmitted and reflected *P* and *S* body waves from local earthquakes near or within the FZ (Li *et al.* 2007). Fig. 3 shows a synthetic waveform record section for an earthquake located west of a hypothetic FZ. We set up the FZ model with a width of 300 m and velocity drop of 40 per cent in both $V_p$ and $V_s$. The FZ has a N–S orientation and the seismic array is perpendicular to the strike. Because of the low-velocity FZ, the direct *P* and *S* arrivals at the eastern stations are increasingly delayed starting from the station located at the western boundary of the FZ (Fig. 3). Besides the direct *P* and *S* waves, multiple internal *P* and *S* reflections from boundaries of the FZ are also shown in Fig. 3. Their corresponding ray paths are shown on the left-hand side. Here we label them as $P^2$, $S^2$, $P^4$, $S^4$ and so on, where the superscript indicates the number of additional ray path legs in the FZ. For stations located outside the FZ, the multiple reflections show little moveout relative to the direct arrivals. For stations located within the FZ, the forward and backward reflections at the boundaries of the FZ have the opposite traveltime moveouts, forming a characteristic 'V'-shaped pattern (Fig. 3). In contrast, the traveltime patterns for an earthquake located in the FZ are drastically different. Fig. 4 shows a record section for an event located in the hypothetic FZ. For stations in the FZ, the direct *P* and *S* arrivals are delayed and the delays from the opposite reflections from the FZ boundaries have the opposite moveouts, forming a distinctive 'X'-shaped pattern.

In both cases, the delays of the direct *P* and *S* arrival times start from stations at the FZ boundaries. Therefore, we can constrain the width of the LVZ directly. The differential arrival times between the direct and FZ-reflected *P* and *S* waves (labelled $P^2$ and $S^2$ in Fig. 3) are used to determine the velocity drops of the LVZ compared to the host rock. When the event is close to the FZ, the differential times can be expressed as

$$t_{P^n} - t_P = nw\sqrt{V_p^{-2} - p^2}, \tag{1}$$

$$t_{S^n} - t_S = nw\sqrt{V_s^{-2} - p^2}, \tag{2}$$

where $p$ is the ray parameter, $V_p$ and $V_s$ are *P* and *S* velocities in the FZ, and $n$ is the number of ray legs of the multiple reflection in the FZ. Using the new technique, the trade-off between the LVZ width and velocity reduction is greatly reduced (Li *et al.* 2007). The method has, however, some limitations. For example, events have to be close to seismic stations so that the free-surface effect can be easily corrected. To use generalized ray theory, we have to ignore depth-dependent variations of host-rock and LVZ structures. When such depth-dependent variations are evident, we use the finite-differences method in the modelling.

Fig. 5 shows a waveform record section from event 3025 located on the southwestern side of the Calico fault trace. Both the direct *P*- and *S*-wave arrivals are increasingly delayed starting near station B07 and ending near station B21 (Fig. 5). The increased delays occur over a distance of ∼1.3 km, indicating existence of a LVZ with its northeastern boundary near B07 and southwestern boundary near B21. This allows us to constrain the LVZ width to be ∼1.3 km. Fig. 6 shows another waveform record section from event 3429 located in the Calico FZ (Fig. 1). The direct *P*- and *S*-wave arrivals are delayed between station B08 and B21. FZ-reflected *P*- and *S*-wave arrival

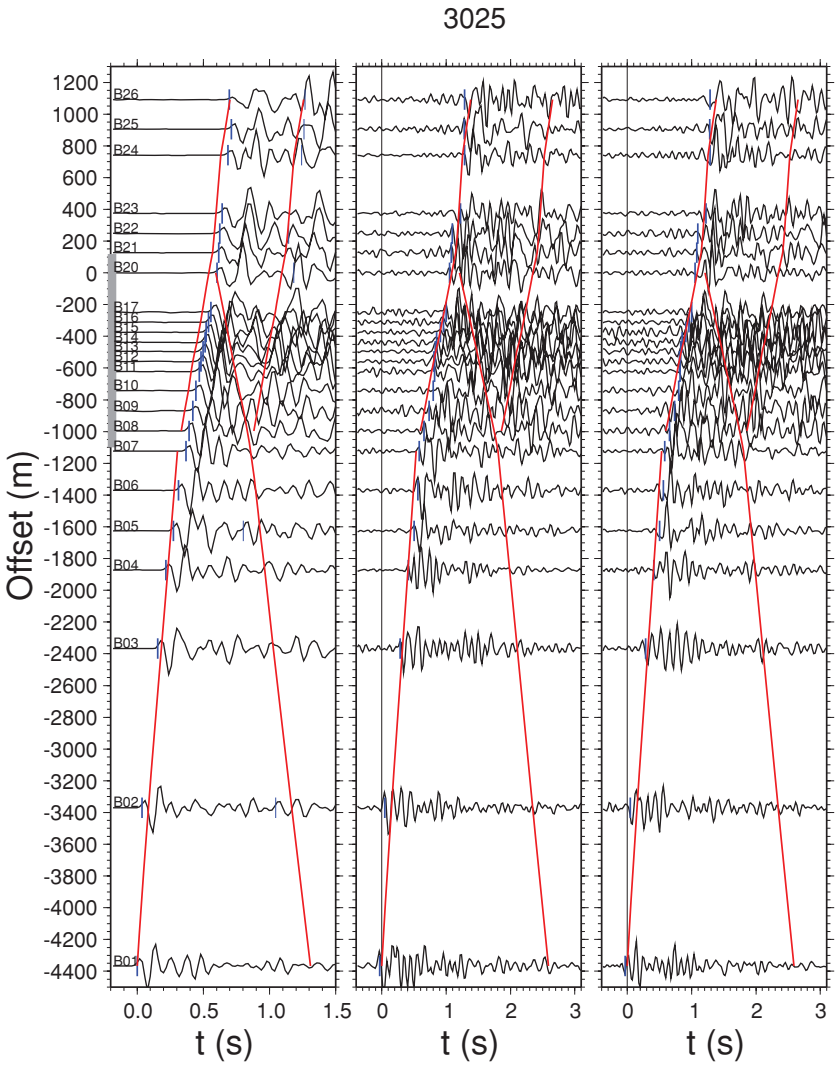


**Figure 5.** From left to right are vertical, radial, and tangential components of waveforms from an event 3025. The vertical component is in the *P* time window and the radial and tangential components are in the *S* window. The Y axis is the offset from the reference station of the array B (Fig. 1) from southwest to northeast. Blue line shows the hand-picked direct *P*- and *S*-wave arrivals. Blue vertical bars denote the FZ-reflected arrivals. Red lines represent the direct and FZ-reflected *P* and *S* arrivals based on a 1-D vertical LVZ model (width and velocity drop obtained in this study). Grey bar shows location of the LVZ.

times show a typical 'X' arrival time pattern for an event located in the FZ (Fig. 4), which confirms the existence of a ∼1.3 km wide LVZ.

We identified the FZ-reflected *P* and *S* waves at some stations (Fig. 5). The differential traveltimes between the direct and the FZ-reflected *P* and *S* phases were used to determine the velocities in the FZ. We computed theoretical arrival times of the direct and FZ-reflected waves for a simple 1-D FZ model in which we fixed the $V_p$ of host rock to be 6.3 km s$^{-1}$ and the $V_s$ to be 3.6 km s$^{-1}$, as this simple model approach was justified in previous studies (Li *et al.* 2007; Yang & Zhu 2010b). The best-estimated LVZ *P*-wave velocity drop is 40 per cent and *S*-wave velocity drop is 50 per cent relative to the host rock. The model-predicted arrival times of the direct and FZ-reflected waves are shown in Figs 5 and 6.

### 3.2 LVZ dip and depth extents

In a previous study of the San Jacinto FZ (Yang & Zhu 2010b), we determined the dip of the FZ using differential arrival times between the northeastern most and southwestern most stations of the array. However, we could not constrain the Calico FZ dip using the same analysis because there are gaps in event distributions, particularly on the northeastern side of the FZ (Fig. 8). The gaps lead to a large uncertainty of the dip of the FZ, from 60° to 90°. Therefore, we had to start with a vertical LVZ model, as suggested by previous study of FZ trapped waves and traveltime tomography (Cochran *et al.* 2009). Using the vertical FZ model with the best-estimated FZ width and velocity contrasts, the model-predicted direct *P* and *S* arrivals agree well with observed arrival times for earthquakes located on the southwestern side of the fault (Fig. 5) and events in the FZ (Fig. 6). But there are notable differences between the model-predicted and observed arrival times for earthquakes located on the northeastern side of the fault. Fig. 7 shows the record section of event 4843 located on the northeastern side of the fault (Figs 1 and 8). *P* and *S* arrival times are earlier than predicted by the 1-D vertical FZ model from stations B09 to B01.

We tried to constrain the LVZ dip by modelling the direct *P* arrivals. Fig. 9 shows the direct *P*-wave arrival times of two events, event 2055 on the southwestern and event 4843 on the northeastern

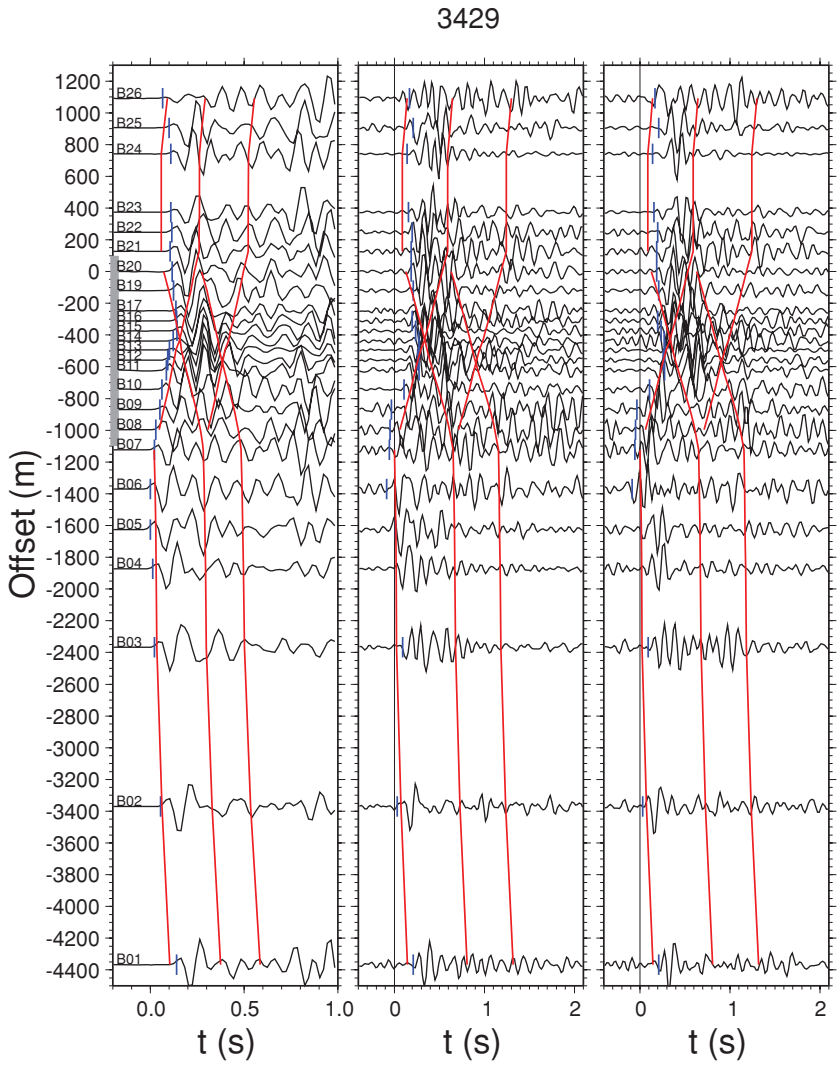


**Figure 6.** From left to right are vertical, radial, and tangential components of waveforms from an event 3429. The vertical component is in the *P* time window and the radial and tangential components are in the *S* window. The *Y* axis stands for the offset from the reference station of the array B (Fig. 1) from southwest to northeast. Blue line shows the hand-picked direct *P*- and *S*-wave arrivals. Red lines represent the direct and FZ-reflected *P* and *S* arrivals based on a 1-D vertical LVZ model. Grey bar shows location of the LVZ.

side of the FZ. Also shown in the figure are the predicted direct *P* arrival times for different FZs dipping from 60° to 100°. For event 2055 on the southwestern side of the FZ, all model predictions agree well with the observed *P* arrival times. Among the four models, the 70° and 80° are slightly better. For event 4843 on the northeastern side of the FZ, all models predict similar arrivals that agree with the observed arrival times at northeastern stations only. The earlier-than-predicted *P* arrival times at stations on the northeastern side of the FZ indicate that the LVZ depth is limited such that *P* and *S* waves from the event can arrive at the stations on the other side of the FZ without going through the LVZ.

We used a 3-D finite-difference code (Graves 1996) to compute the direct *P* and *S* arrival times for vertical LVZ models with different cut-off depths. We performed a grid search for the best dip and depth extent of the LVZ. The dip angle was varied from 60° to 90° at a step of 5°, and the LVZ cut-off depth was searched from 2 to 6 km with a step of 1 km. All other FZ parameters such as width, velocity contrast, and western boundary were fixed as determined in previous section. Fig. 10 shows the rms of weighted *P*-wave traveltime residuals of events on both sides of the FZ (2055, 3429 and 4843) for different dips and depth extents. It can be seen that the vertical FZ can be definitely ruled out because of the large rms of traveltime residuals, no matter what cut-off depth is used, as reported by previous study of Yang & Zhu (2010a). The best-estimated depth for the LVZ is ∼3 km and the LVZ dips 70° northeast, as constrained by the rms contour (Fig. 10). The contour shows a slight trade-off between the LVZ depth and dip. Comparisons of the observed and model-predicted arrival times for a 70°-dip LVZ with different depths are shown in Fig. 11, which suggests that the uncertainties of the LVZ depth extent are ±1 km. Fig. 12 shows the observed and model-predicted arrival times for a 3-km-deep LVZ with different dip angles. Thus we estimated the uncertainties of the LVZ dip are ±5°.

## 4 DISCUSSION AND CONCLUSIONS

In this study, we investigated the Calico FZ structure by modelling traveltimes of local earthquake body waves recorded by a temporary array. Using a recently developed technique, we found a

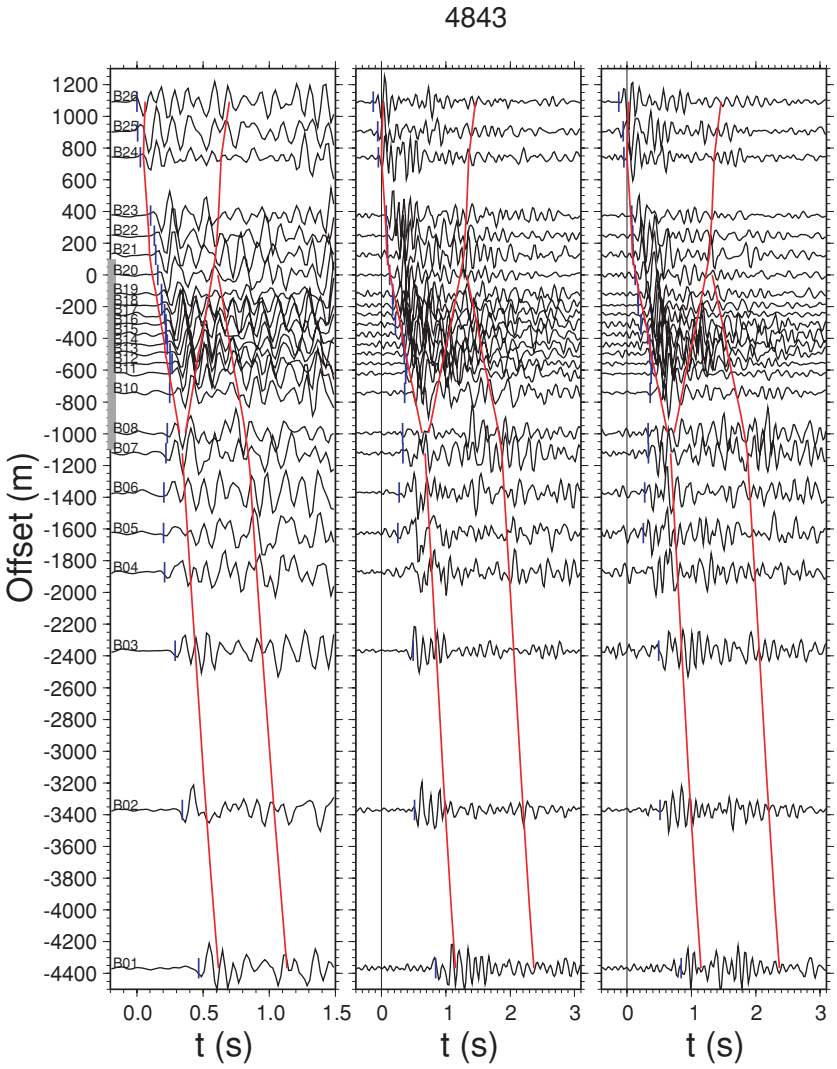


**Figure 7.** From left to right are vertical, radial, and tangential components of waveforms from an event 4843 located on the northeastern side of the FZ (Fig. 8). The vertical component is in the *P* time window and the radial and tangential components are in the *S* window. The *Y* axis stands for the offset from the reference station of the array B (Fig. 1) from southwest to northeast. Blue line shows the hand-picked direct *P*- and *S*-wave arrivals. Red lines represent the direct and FZ-reflected *P* and *S* arrivals based on a 1-D vertical LVZ model. Grey bar shows location of the LVZ.

1.3-km-wide LVZ along the Calico fault. Seismic velocities of the LVZ are reduced 40 per cent in $V_p$ and 50 per cent in $V_s$, consistent with previous study of the Calico fault using FZ trapped waves (Cochran *et al.* 2009). Based on a systematic analysis of travel-times of events from both sides of the fault, we found the LVZ is not vertical but dips 70° northeast. In addition, the LVZ extends to 3 km in depth, shallower than the previous estimate of >5 km using trapped waves of a single event assuming the LVZ is vertical (Cochran *et al.* 2009). The different LVZ dip may lead to a trade-off in estimating the LVZ depth, which may reflect the difference in estimated LVZ depth between this study and the previous work. We interpret the LVZ to be a region of mechanically damaged rocks related to the cumulative effect of past ruptures (e.g. Cochran *et al.* 2009). Considering the low modern seismicity and lack of large historic earthquakes along the Calico fault, the damage zone must have persisted for thousands of years or longer.

The LVZ of the Calico fault is much wider than the neighbouring Landers and Hector Mine faults, 1.3 km versus 200 m (Li *et al.* 1994, 2002, 2003; Peng *et al.* 2003; Li *et al.* 2007), and other crustal faults studied using seismic waves. For instance, damage zone widths of the SAF at Parkfield were estimated ∼150 m from modelling trapped waves (Li *et al.* 2004; Lewis & Ben-Zion 2010; Wu *et al.* 2010). The Karadere-Duzce branch of the North Anatolian fault was estimated to have a LVZ of thickness in order of ∼100 m (Ben-Zion *et al.* 2003). The San Jacinto FZ was documented to have LVZs of ∼100–150 m wide (Li & Vernon 2001; Lewis *et al.* 2005; Yang & Zhu 2010b). Effects of the LVZ width on rupture propagation were shown in a recent numerical simulation in which they found that the LVZ width can affect the rise time of slip and there is a transition from pulse-like rupture to crack-like rupture as the width increases (Huang & Ampuero 2010). Thus, rupture propagation pattern for earthquakes occurring on the Calico fault might be significantly different compared to the Landers and Hector earthquakes.

By investigation of the development of fracture distributions as a function of displacement, Savage & Brodsky (2011) suggested that

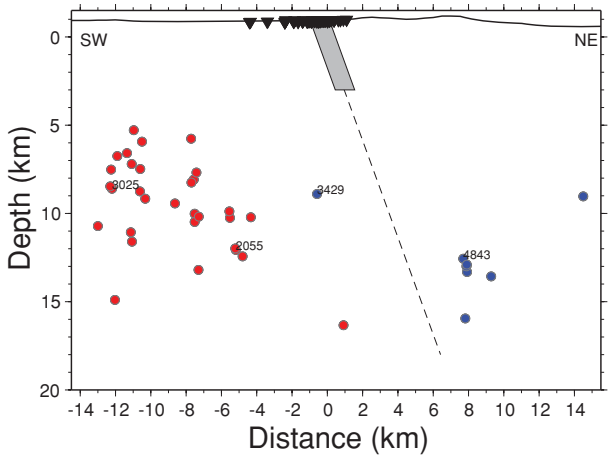


**Figure 8.** A cross-section view of event locations (colour dots) and stations (triangles). Blue and red colours represent positive and negative *P*-wave traveltime differences between the northeastern most and southwestern most stations of the B array, respectively. Grey bar shows the dip and depth of the low-velocity zone obtained in this study.

the width of a damage zone is proportional to the total displacement accumulated along the fault. However, their data points are plotted under log–log scale making it difficult to distinguish between a FZ width of 200 m versus 1.3 km. In fact, the width of the Calico FZ is one order of magnitude larger than the widths of the LVZs of the Landers and Hector Mine faults. The large difference may due to that the Calico fault is a more mature fault, while the Landers and the Hector Mine FZs are relatively new. Furthermore, the temporary array deployment across the Landers and Hector Mine faults were probably initiated to capture the damage caused by the most recent ruptures, thus previous reports may focus on narrow zones that were highly damaged following a large earthquake (Cochran *et al.* 2009). In addition, the Calico fault has a fairly complex structure, which may explain the relatively lower quality observations of FZ-reflected phases in this study, compared to the data from the temporary seismic experiment following the 1992 Landers earthquake. The Calico fault experienced multiple step-overs in geological history (U.S. Geological Survey & California Geological Survey 2006). As shown in Fig. 2, the array is located along a branched portion of the fault. It is likely that material between the fault strands is more highly damaged as has been observed in dynamic modelling of geometrically complex faults (e.g. Duan & Day 2008). The wide damage zone of the Calico fault may also result from low confining pressure across

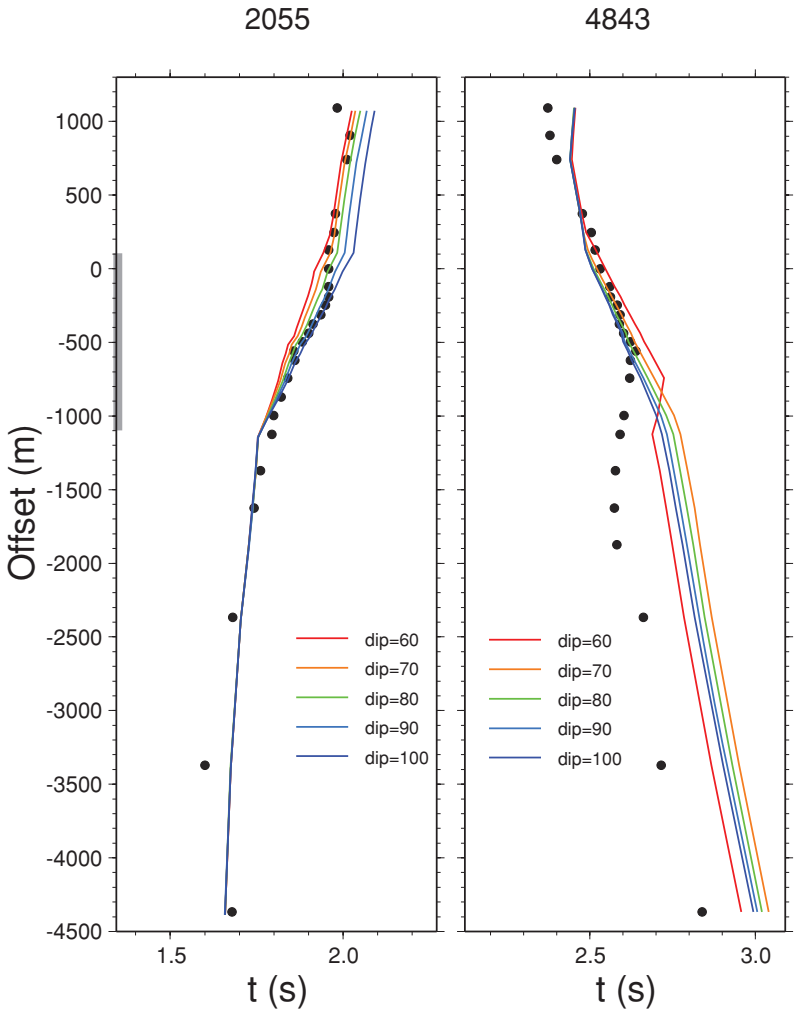


**Figure 9.** *P* wave arrival times (dots) and predictions of different dipping models (lines) for events on the southwestern and the northeastern side of the FZ. Grey bar shows location of the LVZ.

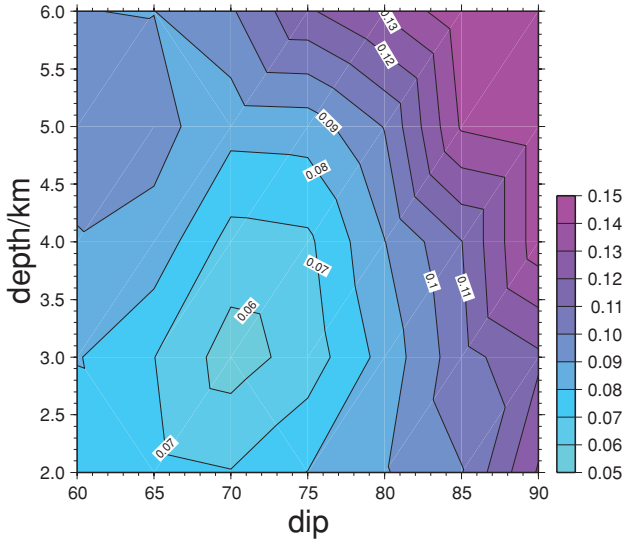


**Figure 10.** RMS of traveltime residuals in sec. for different dips and cut-off depths of LVZ.

the fault. Usually a portion of the damaged zone resulting from a large earthquake heals due to stress accumulation after the event, as reported by Li *et al.* (1998) after the 1992 Landers earthquake. But if the confining pressure across the fault is low, there will be less amount of healing and the width of the damaged zone increases with time. Using dynamic rupture models, Duan (2010) and Duan *et al.* (2011) suggested that inelastic deformation signals along FZs may be used to constrain the stress state in the crust. Therefore, the above hypothesis could be tested using geodetic measurement of FZ response to nearby earthquakes.

Some seismic studies have suggested that the fault damage zone extends to great depth, >10 km (Li *et al.* 2002; Li *et al.* 2003; Wu *et al.* 2010). In this study, we found a 3 km deep LVZ along the Calico fault by analysis of arrival time advances at stations on one side of the fault from earthquakes on the other side. During the analysis, we fixed the LVZ strike, dip, velocity contrast and width, and event locations, and estimated the LVZ depth uncertainty to be ∼1 km (Fig. 11). The uncertainty of LVZ depth could be very large considering the combined effect of the uncertainties of FZ parameters. One possible improvement is to analyse such arrival time advances for a large number of events from both sides of the fault, especially events close to the FZ, so that the LVZ dip and depth could be well constrained simultaneously. Unfortunately, most local earthquakes recorded in the Calico experiment were from one side and were not that close to the FZ (Fig. 1).

As documented here, we found a 1.3-km-wide LVZ with 40 per cent reduction in $V_p$ and 50 per cent reduction in $V_s$ along the Calico fault, southern California, by modelling high frequency body waves of local earthquakes. The LVZ dips 70° northeast and its depth extent is 3 km.

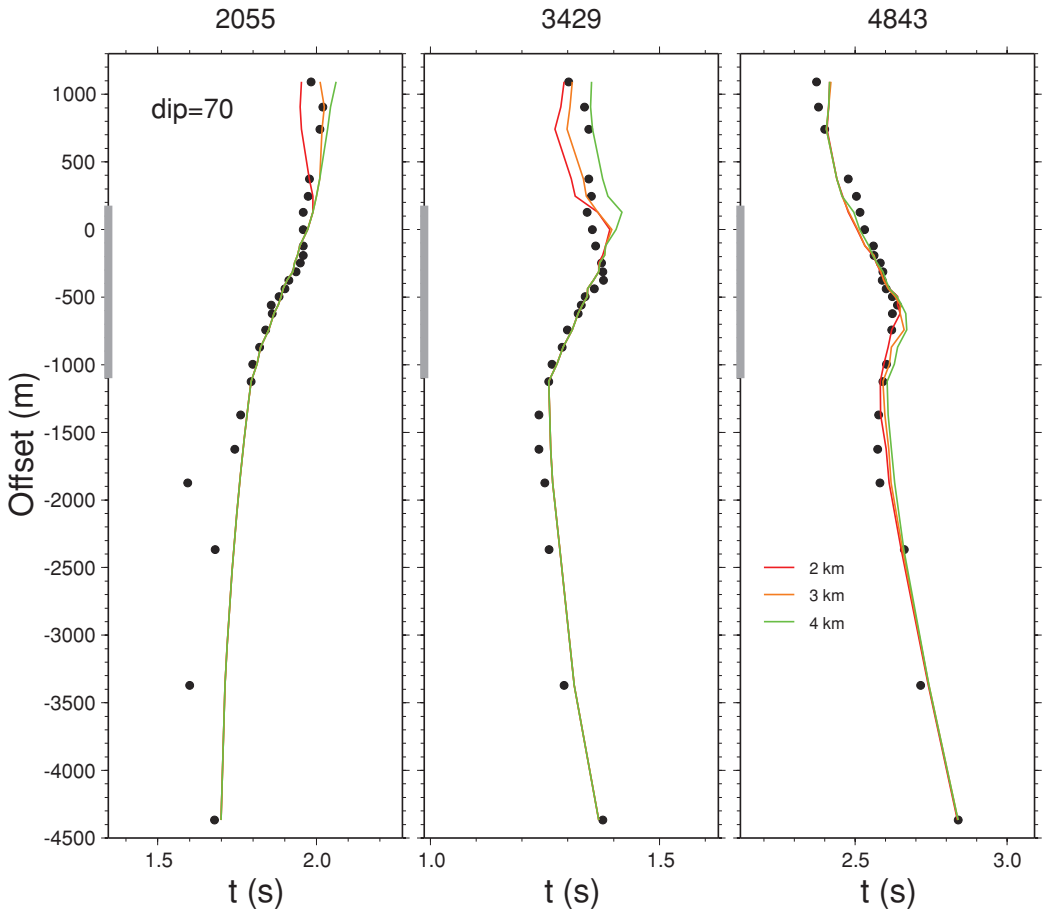


**Figure 11.** Observed (dots) and model-predicted *P* arrival times (lines) for event 2055, event 3429 and event 4843 for a 70°-dip LVZ. Colours correspond to different LVZ depths.

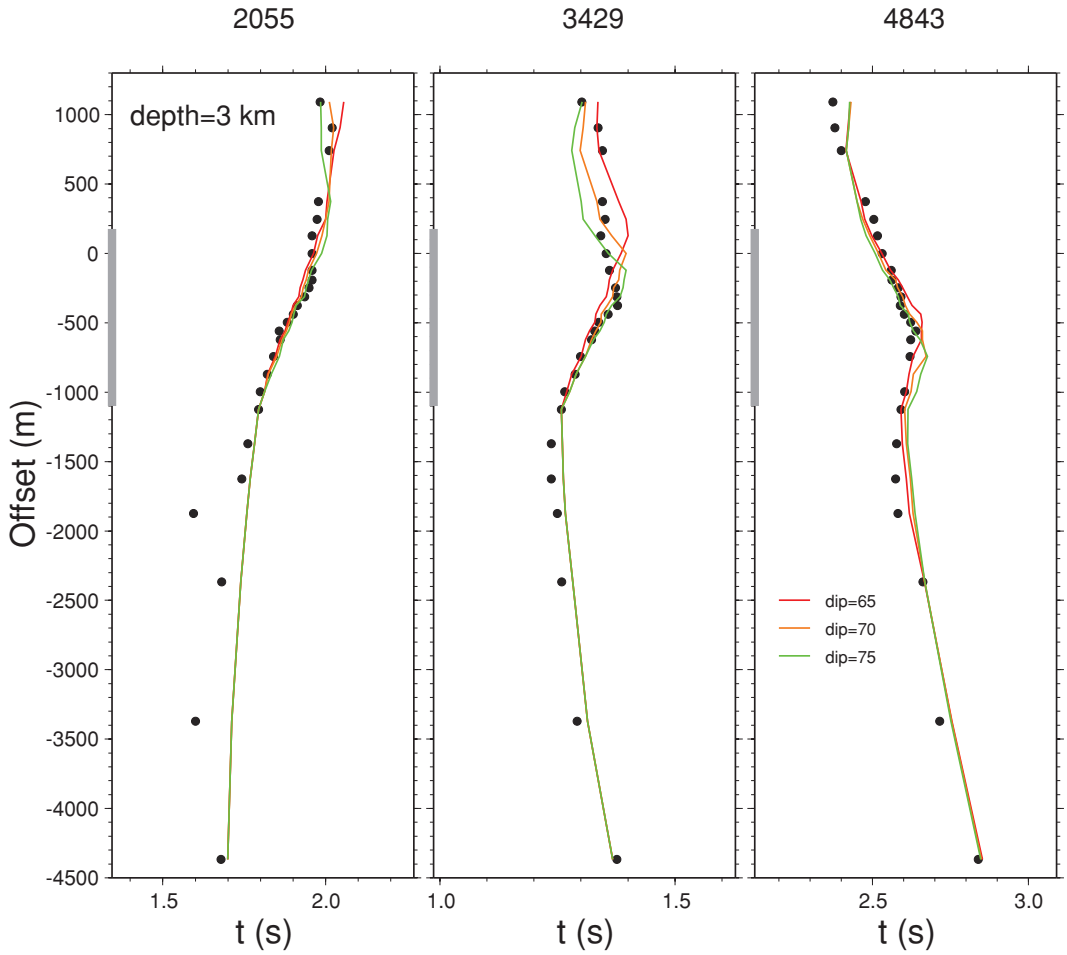


**Figure 12.** Observed (dots) and model-predicted *P* arrival times (lines) for event 2055, event 3429 and event 4843 for a 3-km-deep LVZ. Colours correspond to different LVZ dips.

## ACKNOWLEDGMENTS

The authors thank editor Dr. Yehuda Ben-Zion and two anonymous reviewers for their constructive comments that greatly improve the manuscript. The authors benefit from discussions with Dr. Yajing Liu and Dr. Jian Lin of Woods Hole Oceanographic Institution, and thank Dr. Liu's support of the high-performance workstation for the finite-difference computation. This work is supported by the National Science Foundation under Grant No. EAR-0609969 and EAR-0838195.

## REFERENCES

Aki, K., 1979. Characterization of barriers on an earthquake fault, *J. geophys. Res.,* **84**, 6140–6148.

Ben-Zion, Y. & Aki, K., 1990. Seismic radiation from an SH line source in a laterally heterogeneous planar fault zone, *Bull. seism. Soc. Am.,* **80**, 971–994.

Ben-Zion, Y. & Sammis, C., 2003a. Mechanics, structure and evolution of fault zones, *Pure appl. Geophys.,* **166**, 1533–1536, doi:10.1007/s00024-009-0509-y.

Ben-Zion, Y. & Sammis, C.G., 2003b. Characterization of fault zones, *Pure appl. Geophys.,* **160**, 677–715.

Ben-Zion, Y. & Shi, Z., 2005. Dynamic rupture on a material interface with spontaneous generation of plastic strain in the bulk, *Earth planet. Sci. Lett.,* **236**, 486–496.

Ben-Zion, Y. et al., 2003. A shallow fault-zone structure illuminated by trapped waves in the Karadere-Duzce branch of the North Anatolian fault, western Turkey, *Geophys. J. Int.,* **152**(3), 699–717, doi:10.1046/j.1365-246X.2003.01870.x.

Chester, F.M. & Logan, J.M., 1986. Implications for mechanical properties of brittle faults from observations of the Punchbowl Fault zone, California, *Pure appl. Geophys.,* **124**, 79–106.

Chester, F.M., Evans, J.P. & Biegel, R.L., 1993. Internal structure and weakening mechanisms of the San Andreas fault, *J. geophys. Res.,* **98**, 771–786.

Cochran, E.S., Li, Y., Shearer, P.M., Barbot, S., Fialko, Y. & Vidale, J.E., 2009. Seismic and geodetic evidence for extensive, long-lived fault damage zones, *Geology,* **37**, 315–318, doi:10.1130/G25306A.1.

Dokka, R.K. & Travis, C.J., 1990. Late Cenozoic strike-slip faulting in the Mojave desert, California, *Tectonics,* **9**(2), 311–340.

Dor, O., Rockwell, T.K. & Y. Ben-Zion, 2006. Geological observations of damage asymmetry in the structure of San Jacinto, San Andreas and Punchbowl faults in southern California: a possible indicator for preferred rupture propagation direction., *Pure appl. geophys.,* **163**, 301–349.

Duan, B., 2010. Inelastic response of compliant fault zones to nearby earthquakes, *Geophys. Res. Lett.,* **37**, doi:10.1029/2010GL044150.

Duan, B. & Day, S.M., 2008. Inelastic strain distribution and seismic radiation from rupture of a fault kink, *J. geophys. Res.,* **113**, doi:10.1029/2008JB005847.

Duan, B., Kang, J. & Li, Y., 2011. Deformation of compliant fault zones induced by nearby earthquakes: theoretical investigations in two dimensions, *J. geophys. Res.,* **116**, doi:10.1029/2010JB007826.

Eberhart-Phillips, D., Stanley, W.D., Rodriguez, B.D. & Lutter, W.J., 1995. Surface seismic and electrical methods to detect fluids related to faulting, *J. geophys. Res.,* **97**, 12 919–12 936.

Evans, J.P. & Chester, F.M., 1995. Fluid-rock interaction in faults of the San Andreas system: inferences from San Gabriel fault rock geochemistry and microstructures, *J. geophys. Res.,* **100**(B7), 13 007–13 020.

Fialko, Y., Sandwell, D., Agnew, D., Simons, M., Shearer, P. & Minster, B., 2002. Deformation on nearby faults induced by the 1999 Hector Mine earthquake, *Science,* **297**, 1858–1862.

Graves, R.W., 1996. Simulating seismic wave propagation in 3D elastic media using staggered-grid finite differences, *Bull. seism. Soc. Am.,* **86**, 1091–1106.

Hearn, E.H. & Fialko, Y., 2009. Can compliant fault zones be used to measure absolute stresses in the upper crust, *J. geophys. Res.,* **114**(B04403), doi:10.1029/2008JB005901.

Huang, Y. & Ampuero, J.P., 2010. Dynamic slip pulses generated by a damaged fault zone and by fault roughness, *AGU Fall Meeting Abstracts,* 2010.

Kanamori, H., 1994. Mechanics of earthquakes, *Ann. Rev. Earth Planet. Sci.,* **22**, 207–237.

Kanamori, H. & Brodsky, E.E., 2004. The physics of earthquakes, *Rep. Prog. Phys.,* **67**, 1429–1496.

Lewis, M. & Ben-Zion, Y., 2010. Diversity of fault zone damage and trapping structures in the parkfield section of the san andreas fault from comprehensive analysis of near fault seismograms, *Geophys. J. Int.,* **183**, doi:10.1111/j.1365-246X.2010.04816.x.

Lewis, M.A., Peng, Z.G., Ben-Zion, Y. & Vernon, F.L., 2005. Shallow seismic trapping structure in the San Jacinto fault zone near Anza, California, *Geophys. J. Int.,* **162**, 867–881, doi:10.1111/j.1365-246X.2005.02684.x.

Li, H., Zhu, L. & Yang, H., 2007. High-resolution structures of the Landers fault zone inferred from aftershock waveform data, *Geophys. J. Int.,* **171**, 1295–1307, doi:10.1111/j.1365-246X.2007.03608.x.

Li, Y.G. & Vernon, F.L., 2001. Characterization of the San Jacinto fault zone near Anza, California, by fault zone trapped waves, *J. geophys. Res.,* **106**, 30 671–30 688.

Li, Y.G., Leary, P.G., Aki, K. & Malin, P., 1990. Seismic trapped modes in the Oroville and San Andreas fault zones, *Science,* **249**, 763–766.

Li, Y.G., Aki, K., Adams, D., Hasemi, A. & Lee, W.H.K., 1994. Seismic guided waves trapped in the fault zone of the Landers, California, earthquake of 1992, *J. geophys. Res.,* **99**, 11 705–11 722.

Li, Y.G., Vernon, F.L. & Aki, K., 1997. San Jacinto fault-zone guided waves: a discrimination for recently active fault strands near Anza, California, *J. geophys. Res.,* **102**, 11 689–11 701.

Li, Y.G., Vidale, J.E., Aki, K., Xu, F. & Burdette, T., 1998. Evidence of shallow fault zone strengthening after the 1992 *M* 7.5 Landers, California, earthquake, *Science,* **279**, 217–219.

Li, Y.G., Vidale, J.E., Aki, K. & Xu, F., 2000. Depth-dependent structure of the Landers fault zone using fault zone trapped waves generated by aftershocks, *J. geophys. Res.,* **105**, 6237–6254.

Li, Y.G., Vidale, J.E., Day, S.M., Oglesby, D.D. & the, SCEC Field Working Team, 2002. Study of the 1999 M 7.1 Hector Mine, California, earthquake fault plane by trapped waves, *Bull. seism. Soc. Am.,* **92**, 1318–1332.

Li, Y.G., Vidale, J.E., Oglesby, D.D., Day, S.M. & Cochran, E., 2003. Multiple-fault rupture of the *M*7.1 Hector Mine, California, earthquake from fault zone trapped waves, *J. geophys. Res.,* **108**, doi:10.1029/2001JB001, 456.

Li, Y.G., Vidale, J.E. & Cochran, E.S., 2004. Low-velocity damaged structure of the San Andreas Fault at Parkfield from fault zone trapped waves, *Geophys. Res. Lett.,* **31**, L12S06, doi:10.1029/2003GL019, 044.

McClusky, S.C., Bjornstad, S.C., Hager, B.H., King, R.W., Meade, B.J., Miller, M.M., Monastero, F.C. & Souter, B.J., 2001. Present day kinematics of the Eastern California Shear Zone from a geodetically constrained block model, *Geophys. Res. Lett.,* **28**(17), 3369–3372.

McGuire, J. & Ben-Zion, Y., 2005. High-resolution imaging of the Bear Valley section of the San Andreas fault at seismogenic depths with fault-zone head waves and relocated seismicity, *Geophys. J. Int.,* **163**, 152–164, doi:10.1111/j.1365-246X.2005.02703.x.

Oskin, M., Peng, L., Blumentritt, D., Mukhopadhyay, S. & Iriondo, A., 2007. Slip rate of the Calico fault: implications for geologic versus geodetic rate discrepancy in the eastern California shear zone, *J. geophys. Res.,* **112**(B03402), doi:10.1029/2006JB004451.

Peng, Z. & Ben-Zion, Y., 2006. Temporal changes of shallow seismic velocity around the Karadere-Düzce branch of the North Anatolian fault and strong ground motion, *Pure appl. Geophys.,* **163**, 567–600.

Peng, Z., Ben-Zion, Y., Michael, A.J. & Zhu, L.P., 2003. Quantitative analysis of seismic fault zone waves in the rupture zone of the Landers, 1992, California earthquake: evidence for a shallow trapping structure, *Geophys. J. Int.,* **155**, 1021–1041.

Rovelli, A., Caserta, A., Marra, F. & Ruggiero, V., 2002. Can seismic waves be trapped inside an inactive fault zone? The case study of Nocera Umbra, central Italy, *Bull. seism. Soc. Am.,* **92**, 2217–2232.

Sammis, C.G., Rosakis, A.J. & Bhat, H.S., 2009. Effects of off-fault damage on earthquake rupture propagation:experimental studies, *Pure appl. Geophys.,* **166**, 1629–1648, doi:10.1007/s00024-009-0512-3.

Savage, H.M. & Brodsky, E., 2011. Collateral damage: the evolution with displacement of fracture distribution and secondary fault strands in fault damage zones, *J. geophys. Res.,* **116**, doi:10.1029/2010JB007665.

Scholz, C.H., 1990. *The Mechanics of Earthquakes and Faulting,* Cambridge Univ. Press, New York.

Schulz, S.E. & Evans, J.P., 1998. Spatial variability in microscopic deformation and composition of the Punchbowl fault, southern California: implications for mechanisms, fluid-rock interaction, and fault morphology, *Tectonophysics,* **295**, 223–244.

Simons, M., Fialko, Y. & Rivera, L., 2002. Coseismic deformation from the 1999 $M_w$ 7.1 Hector Mine, California, earthquake as inferred from InSAR and GPS observations, *Bull. seism. Soc. Am.,* **92**, 1390–1402, doi:10.1785/0120000933.

U.S. Geological Survey and California Geological Survey, 2006. Quaternary fault and fold database for the United States, accessed Nov. 28, 2010, from USGS web site: http//earthquake.usgs.gov/regional/qfaults, U.S. Geological Survey and California Geological Survey.

Vidale, J.E. & Li, Y.G., 2003. Damage to the shallow Landers fault from the nearby Hector Mine earthquake, *Nature,* **421**, 524–526.

Wu, C., Peng, Z. & Ben-Zion, Y., 2009. Non-linearity and temporal changes of fault zone site response associated with strong ground motion, *Geophys. J. Int.,* **176**, 265–278, doi:10.1111/j.1365-246X.2008.04005.x.

Wu, J., Hole, J.A. & Snoke, J.A., 2010. Fault zone structure at depth from differential dispersion of seismic guided waves: evidence for a deep waveguide on the san andreas fault, *Geophys. J. Int.,* **182**, doi:10.1111/j.1365-246X.2010.04612.x.

Yang, H. & Zhu, L., 2010a. Depth extent of low-velocity fault zones, *EOS, Trans. Am. geophys. Un.,* **91**(52), Fall Meet. Suppl., T33B-2250.

Yang, H. & Zhu, L., 2010b. Shallow low-velocity zone of the San Jacinto fault from local earthquake waveform modelling, *Geophys. J. Int.,* **183**, 421–432, doi:10.1111/j.1365-246X.2010.04744.x.

Yang, H., Zhu, L. & Chu, R., 2009. Fault-plane determination of the 18 April 2008 Mt. Carmel, Illinois, earthquake by detecting and relocating aftershocks, *Bull. seism. Soc. Am.,* **99**(6), 3413–3420, doi:10.1785/0120090038.

Zhang, H., Thurber, C. & Bedrosian, P., 2009. Joint inversion for vp, vs, and vp/vs at SAFOD, Parkfield, California, *Geochem. Geophys. Geosyst.,* **10**(Q11002), doi:10.1029/2009GC002709.

Zhao, P. & Peng, Z., 2008. Velocity contrast along the Calaveras fault from analysis of fault zone head waves generated by repeating earthquakes, *Geophys. Res. Lett.,* **35**, doi:10.1029/2007GL031810.

## SUPPORTING INFORMATION

Additional Supporting Information may be found in the online version of this article:

**Table 1.** Local earthquakes used in this study.

Please note: Wiley-Blackwell are not responsible for the content or functionality of any supporting materials supplied by the authors. Any queries (other than missing material) should be directed to the corresponding author for the article.